COBEM UBERLÂNDIA 2019

ABCM Associação Brasileira de Engenharia e Ciências Mecânicas

25th ABCM International Congress of Mechanical Engineering
October 20-25, 2019, Uberlândia, MG, Brazil

COB-2019-0846
NUMERICAL INVESTIGATION OF THE INFLUENCE OF THE REYNOLDS NUMBER ON THE HEAT TRANSFER OF A VISCOPLASTIC FLUID

Luiz Paulo Borges Miranda
Daniel Dall'Onder dos Santos
Federal University of Uberlândia, Av. João Naves de Ávila 2121, Uberlândia, MG, 38408-100, Brazil
luiz.miranda@ufu.br
dallonder@ufu.br

Abstract. *Non-Newtonian fluids are a constant presence at several industrial applications, so there is interest to understand their behavior to optimize these processes. One of these behaviors with commercial interest is the viscoplastic behavior, characterized by an abrupt change of the apparent viscosity when a certain amount of stress is achieved. The present work performs a study of the influence of the Reynolds number over some flow parameters with industrial interest. The mechanical model is numerically approximated using an OpenFOAM® routine developed by the authors based in the finite volume method. To model the viscoplastic behavior, the SMD model was chosen. The adopted geometry is a planar channel with an expansion followed by an abrupt contraction. The channel walls are kept insulated and the heat transfer occurs only at the expansion-contraction walls. The Reynolds number influence was evaluated adopting two different values of the plastic number (0.4 and 0.6), while the other dimensionless groups were kept constant. The parameters used to compare the analyzed flows were the heat transfer, the pressure drop and the ratio between the area of the apparent unyielded zones and the total area of the cavity. The obtained results show that the mean Nusselt number have a positive correlation with the Reynolds number, while the influence of the cavity over the pressure drop decreases with the increase of the Reynolds number. These results are in accordance with the ones found in the literature.*

Keywords: *viscoplastic behavior; rheological properties; SMD model; heat transfer; expansion and abrupt contraction*

1. INTRODUCTION

It is known that many multiphase and structured fluids such as foams, emulsions and suspensions found in a variety of engineering applications exhibit viscoplastic behavior. Some typical examples are: processed foods and chocolates; toiletries and cosmetics; drilling muds, lubricants and greases; construction materials; among others (Nirmalkar *et al.*, 2014). In these applications, heat transfer and pressure drop are important parameters, as they are used to predict the flow behavior and to estimate the energy necessary for heating and transportation. For several applications, the temperature and the presence of stationary apparent unyielded zones can compromise the quality of the fluid, changing the properties of the fluid and creating fouling layers.

The heat transfer in viscoplastic systems differs significantly from that in Newtonian fluids or in purely viscous fluids without a yield stress: the coexistence of the fluid-like (yielded) and solid-like (apparently unyielded) regions in the flow affect the characteristics of the flow and the heat transfer mechanisms. To understand this phenomenon, several studies have been developed, for different configurations: Turan *et al.* (2011) simulated two-dimensional steady-state natural convection in rectangular enclosures with differentially heated side walls for a range of different aspect ratios of the enclosure, Rayleigh numbers, and Bingham numbers. Raja *et al.* (2015) investigated the flow of Bingham fluids past a two-dimensional heated flat plate over a range of Reynolds numbers, Prandtl numbers, and Bingham numbers. Nirmalkar *et al.* (2014) solved numerically the equations of motion and energy for the laminar free convection heat transfer from a horizontal heated cylinder to a Bingham plastic fluid over a range of imposed conditions like the Rayleigh number, the Prandtl number, and the Bingham number. Shyam and Chhabra (2013) have developed a numerical solution for the momentum and heat transfer characteristics of a heated cylinder of square cross-section immersed in a streaming Bingham plastic medium, imposing the plastic Reynolds number, the Prandtl number, and the Bingham number. Gupta *et al.* (2017) analyzed the laminar forced convection momentum and heat transfer characteristics of a circular disk positioned inside a flow of Bingham plastic fluid and oriented normal to the flow. The disk was modelled by two different conditions: a constant flux and a constant temperature condition. Both conditions were analyzed for a range of Reynolds number, Prandtl number, Bingham number, and for different ratios thickness-to-diameter of the disk.

The model adopted in this work to reproduce the viscoplastic behavior is the one proposed by de Souza Mendes and Dutra (2004). This model is continuous and has continuous derivatives, making it more convenient for numerical simulation and curve fitting procedures. The qualitative behavior is the same as in the most of the viscoplastic fluids of interest: a high viscosity plateau for low stress, followed by a sharp drop in the viscosity level and then a power-law region (de Souza Mendes and Dutra, 2004). When simulating pseudoplastic fluids, a new term is introduced to prevent the apparent viscosity tending to zero when the shear rate tends to infinity. Concearning viscoplaticity modeling using the SMD equation, the expansion-contraction axisymmetric channel was studied by de Souza Mendes *et al.* (2007), where experimental results were compared with numerical simulations, obtained with the condition of Reynolds number lower than 0.1. Hermany (2012) also studied the expansion-contraction axisymmetric channel, simulating flows where the inertia forces are not negligible, with a rheological Reynolds number ranging from 0.5 to 25. Naccache and Barbosa (2007) compares the numerical simulation of an expansion-contraction planar channel with experimental results. These three works mentioned above only solve the mass and momentum balance equations. The influence of the Reynolds number over the heat transfer and others parameters of interest were studied by the present work, using an OpenFOAM® routine developed by the authors to solve non-Newtonian incompressible steady-state flows. The numerical code uses the SIMPLE algorithm to solve the balance equations using the finite volume method.

2. METHODOLOGY

2.1 Mechanical model

The fluid is assumed incompressible and the flow is at steady state. The mass, momentum and energy balance equations can be expressed as, respectively

$$\begin{aligned} &\nabla \cdot \mathbf{u} = 0 \\ &\rho(\nabla \mathbf{u})\mathbf{u} = -\nabla p + \nabla \cdot \boldsymbol{\tau} \\ &\rho c_p(\nabla T)\mathbf{u} = \kappa \nabla^2 T \end{aligned} \tag{1}$$

where $\boldsymbol{u}$ is the velocity vector, ρ is the specific mass of the fluid, p is the hydrostatic pressure, c_p is the fluid specific heat, T is the temperature and κ is the thermal conductivity. c_p and κ are considered constants. $\boldsymbol{\tau}$ is the extra-stress tensor, and it is defined by the constitutive equation, as follows:

$$\boldsymbol{\tau} = 2\eta(\dot{\gamma})\mathbf{D}(\mathbf{u}) \tag{2}$$

where $\mathbf{D}(\mathbf{u})$, $\eta(\dot{\gamma})$ and the shear rate $\dot{\gamma}$ are defined as:

$$\mathbf{D}(\mathbf{u}) = \frac{1}{2}(\nabla \mathbf{u} + \nabla \mathbf{u}^T) \tag{3}$$

$$\eta(\dot{\gamma}) = \left[1 - exp\left(\frac{-\eta_0}{\tau_0}\dot{\gamma}\right)\right]\left(\frac{\tau_0}{\dot{\gamma}} + K\dot{\gamma}^{n-1}\right) + \eta_\infty \tag{4}$$

$$\dot{\gamma} = \sqrt{2tr\mathbf{D}(\mathbf{u})^2} \tag{5}$$

where η_0 and η_∞ are, respectively, the viscosities for very low and high values of the shear rate $\dot{\gamma}$, τ_0 is the yield stress limit of the material, K is the consistency index and n is the power-law index. Equation (4) represents the SMD model, and shows that $\eta(\dot{\gamma})$ is function of the shear rate, but it is independent of the temperature.

2.2 Dimensionless groups of interest

In this work, the dimensionless groups of interest are: the Reynolds number, the Prandtl number, the jump number, the plastic number and the Nusselt number. The expressions for the Reynolds number (*Re*), the Prandtl number (*Pr*) and plastic number (*Pl*) adopted are the definitions proposed by Thompson and Soares (2016), as follows:

$$Re = \frac{\rho {V_c}^2}{\tau_0 + K(\frac{V_c}{L_c})^n + \eta_\infty(\frac{V_c}{L_c})} \tag{6}$$

$$\frac{1}{Pr} = \frac{K(\frac{V_c}{L_c})^n + \eta_\infty(\frac{V_c}{L_c})}{\tau_0 + K(\frac{V_c}{L_c})^n + \eta_\infty(\frac{V_c}{L_c})} \frac{\rho\alpha}{K(\frac{V_c}{L_c})^{n-1} + \eta_\infty} \tag{7}$$

$$Pl = \frac{\tau_0}{\tau_0 + K(\frac{V_c}{L_c})^n + \eta_\infty(\frac{V_c}{L_c})} \tag{8}$$

where α is the thermal diffusivity, V_c and L_c are the characteristic velocity and the characteristic length, respectively taken as the value of the velocity at the inlet and the channel height (*H1*).

The jump number (*J*) is an dimensionless group proposed by de Souza Mendes *et al.* (2007) that gives a relative measure of the shear rate jump that occurs at $\tau = \tau_0$ and its expression is:

$$J = \frac{\eta_0 \dot{\gamma}_1}{\tau_0} - 1 \tag{9}$$

where $\dot{\gamma}_1 = \left(\frac{\tau_0}{K}\right)^{\frac{1}{n}}$.

The dimensionless apparent viscosity for high shear rates is defined as:

$$\eta^*_\infty = \frac{\eta_\infty \dot{\gamma}_1}{\tau_0} \tag{10}$$

The head loss Hl and the displacement efficiency Φ_{de} are defined as:

$$Hl = \frac{\Delta p_s - \Delta p_c}{\rho(\dot{\gamma}_1 H_1)} \tag{11}$$

$$\Phi_{de} = 1 - \frac{V_{c,0}}{V_c} \tag{12}$$

where Δp_c is the pressure drop calculated between any point of the upstream and downstream channel where the flow is fully developed, Δp_s is the pressure obtained at the same point where Δp_c is obtained, but in a channel without the cavity. To obtain Δp_s, a numerical method was used to solve the balance equations with the fully developed flow conditions. $V_{c,0}$ is the area of the apparent unyielded zones inside the cavity, and V_c is the total area of the cavity.

The Nusselt number (*Nu*) and average Nusselt ($\overline{Nu}$) are equal to:

$$Nu = \frac{L_c}{|T_{wall} - T_{ref}|} \left.\frac{\partial T}{\partial x}\right|_{wf} \tag{13}$$

$$\overline{Nu} = \frac{1}{S_{Nu}} \int_{S_{Nu}} Nu \, dS \tag{14}$$

where S_{Nu} is the surface where $\overline{Nu}$ is calculated, T_{wall} is the wall temperature and T_{ref} is the reference temperature. In this work, S_{Nu} are the cavity walls and $T_{ref} = 0$. The subscript *wf* indicates that $\partial T/\partial x$ is evaluated at the contact between the fluid and the walls.

The dimensionless position vector ($\mathbf{x}^*$), the dimensionless velocity ($\mathbf{u}^*$), the dimensionless pressure (p^*) and the dimensionless temperature (θ) are defined according to the following expressions:

$$\mathbf{x}^* = \frac{\mathbf{x}}{L_c} \qquad \mathbf{u}^* = \frac{\mathbf{u}}{\dot{\gamma}_1 L_c} \qquad p^* = \frac{p}{\tau_0} \qquad \theta = \frac{T - T_C}{T_H - T_C} \tag{15}$$

where T_C is the fluid temperature at the inlet region and T_H is the cavity walls temperature, and $T_H > T_C$.

At the present work, the influence of the Reynolds number is evaluated adopting two different values for the plastic number, equal to 0.4 and 0.6. The other dimensionless numbers are kept constant and equal to *Pr=14.02; J=*10^4*; n=0.5;* η^*_{inf}*=0.01*.

2.3 Geometry and boundary conditions

The flow is along a planar channel, following the dimensions shown in Fig. 1. The ratio between dimension H_2 (cavity height) and dimension H_1 (channel height) is equal to 6.3. The ratio of the length of the cavity (L_2) to the height of the cavity (H_2) is equal to 1 and the ratio of the length L_1 (length of the channel) and H_1 is equal to 16.85. Thus, the analyzed domain has a total length of 40 H_1.

To reduce the computational effort, only half geometry is simulated, with the symmetry line at y^*=0, as shown in Fig. 1. The velocity boundary conditions were impermeability and no-slip on the channel and cavity walls and a flat horizontal velocity profile at the inlet. At the outlet, pressure profile was considered constant. The channel walls were

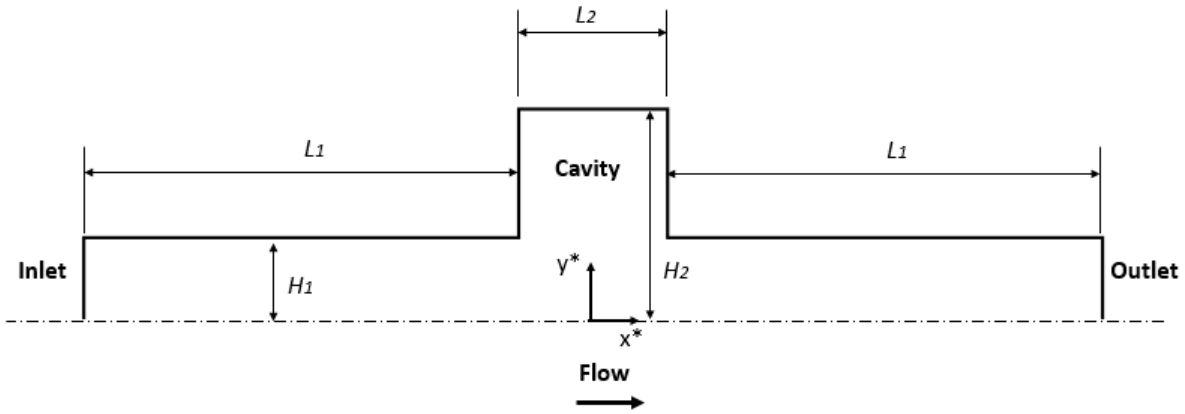

Figure 1. Geometry of the planar channel.

considered thermally insulated. The fluid dimensionless temperature at the inlet is equal to 0 and at the cavity walls is equal to 1.

The mesh is structured, and its elements can be divided in two main groups: one group contains the elements inside the cavity and at the channel bellow it, and the other group consists of the elements inside the inlet and outlet channels. The first group has ideally square elements, and the second has rectangular elements with the ratio height:length equals to 1:2. The final proportions may change a little to fit the dimensions of the geometry domain. By this way, it is possible to define the whole mesh by choosing a theoretical dimensionless element height, h^*_{teo}.

The mesh quality was verified using a methodology proposed by Celik (2008). To ensure that the mesh is fine enough to accurately represent the studied parameters, several tests were made for different critical conditions. The meshes used to test the mesh quality are described at Tab. 1, and the result can be found in Tab. 2, where ϕ_{ext} is the extrapolated value of ϕ and is defined as $\phi_{ext} = (r_{21}^{a_c} * \phi 1 - \phi_2)/(r_{21}^{a_c} - 1)$, *r* is the ratio between the representative length of a element from two different grids, a_c is the theoretical order of accuracy and e_{ext} is the extrapolated relative error. In this work, $a_c = 2$. For the mesh quality tests, the analyzed conditions were the maximum and minimum values of the analyzed range of Re ($Re = 0.1$ and $Re = 50$) , with $Pl = 0.4$.

Table 1. Number of elements and h^*_{teo} of meshes adopted for the mesh quality test procedures.

Mesh	3	2	1
Number of elements	2044	4542	10304
h^*_{teo}	0.1687	0.1125	0.075

Three parameters were adopted to evaluate the mesh quality: $\overline{Nu}$, $|\mathbf{u}^*|_{x^*=0}$ and Δp^*_{10}. Δp^*_{10} is the difference of the dimensionless pressure between the points $(x^*, y^*) = (-10, 0)$ and $(x^*, y^*) = (10, 0)$. $|\mathbf{u}^*|_{x^*=0}$ is the profile of velocity magnitude over the axis $x^* = 0$: a thousand equally spaced points were chosen between $y^* = 0$ and $y^* = 6.3$, and for every point, the mesh quality test was applied, and then the e_{ext} of the profile were evaluated as the weighted average of e_{ext} of each point, adopting the the finer mesh velocity magnitude as the weight function. This procedure was needed to guarantee that velocity profile was evaluated as a whole. As can be seen in Tab. 2, all the obtained e_{ext} were bellow 3%.

3. RESULTS

3.1 Influence of Reynolds number

To analyze the effect of the Reynolds number over the flow, simulations were performed ranging it from 0.1 to 50, adopting two different values for the plastic number (0.4 and 0.6), while the others dimensionless groups were kept constant. Figure 2 shows the profile of the dimensionless velocity magnitude over the y^* axis, for $Pl = 0.4$. With this configuration, for $Re > 20$, the dimensionless velocity magnitude has a considerable increase after $y^* = 2$, indicating the presence of a recirculation zone inside the cavity. Theoretically, every flow has at least one recirculation zone inside the cavity, and maybe more than one. However, the high viscosity plateau for low shear rates, characteristic of the viscoplastic behavior, can prevent these recirculation zones from actually flow. This effect can be seen at the Fig. 2, where even for $Re < 10$ the dimensionless velocity profile shows an increase of its value inside the cavity, but the magnitude of the dimensionless velocity is still some orders of magnitude below the velocity at the symmetry line, for example. With the increase of the Reynolds number, the recirculation zone is able to surpass the yield stress limit, as can be seen in Fig. 3

Table 2. Results of the mesh quality test for $Re = 0.1$ and $Re = 50$

		$\overline{Nu}$			$\lvert\mathbf{u}^*\rvert_{x^*=0}$			Δp^*_{10}		
	mesh	3	2	1	3	2	1	3	2	1
$Re = 0.1$	ϕ	1.10	1.13	1.15	-	-	-	79.1	75.1	75.1
	ϕ_{ext}	1.16			-			75.2		
	$e_{ext}(\%)$	5.17	2.84	0.83	1.95	2.83	1.25	5.22	0.13	0.05
$Re = 50$	ϕ	10.5	11.2	11.9	-	-	-	84.0	83.1	83.0
	ϕ_{ext}	12.2			-			82.9		
	$e_{ext}(\%)$	13.7	7.68	2.24	5.58	2.67	1.17	1.23	0.26	0.11

and Fig. 4. Increasing the Reynolds number even more, the recirculation zone grows up, until a limit defined by the size of the cavity. In Fig. 3(b), it is clear that there is a recirculation zone inside the cavity, but because of its size and center position, the curve for $Re = 15$ in Fig. 2 almost does not show any evidence of its presence. Figure 4 also highlight the difference between the simulations with $Pl = 0.4$ and $Pl = 0.6$: for $Pl = 0.4$, the simulations with $Re > 15$ exhibit a recirculation zone, but for $Pl = 0.6$ the viscoplastic behavior is stronger and there is no recirculation zone for $Re = 15$ or $Re = 20$.

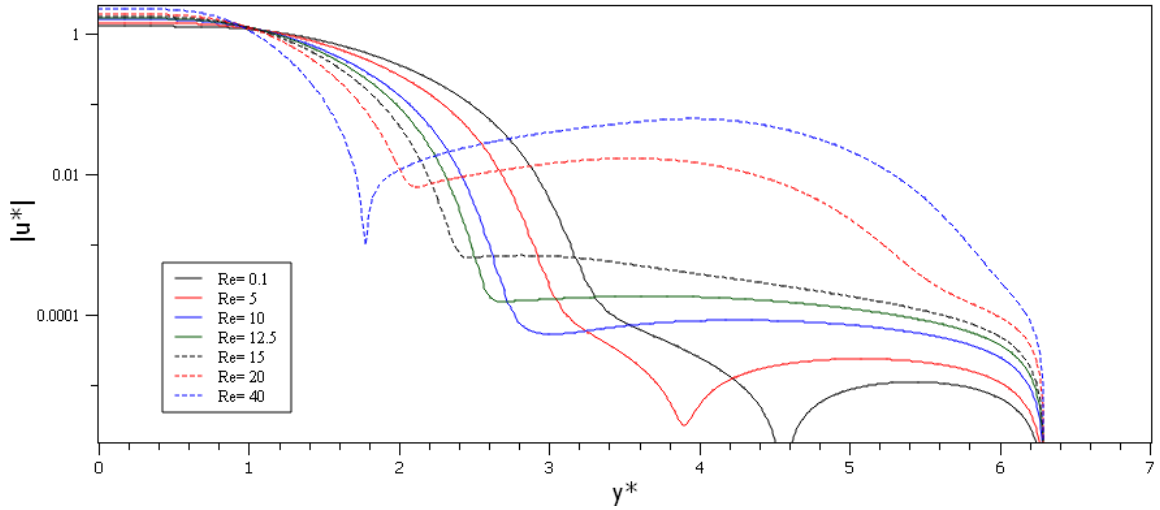

Figure 2. Magnitude of the dimensionless velocity over the y^* axis for different Reynolds numbers at $x^* = 0$, with $Pl = 0.4$.

As can be seen in Fig. 4(b), a new apparent unyielded zone is formed inside the recirculation zone. With this new apparent unyielded zone, there is three different types of apparent unyielded zones in the flow:

- the plug zone: a moving apparent unyielded zone that occurs mainly inside the channel, near the symmetry line.
- the vortex center: a moving apparent unyielded zone that is spinning around a point.
- the stationary apparent unyielded zone: that usually occurs near the cavity walls and corners.

Among the three kinds of apparent unyielded zones, the last two kinds of apparent unyielded zones can be present inside the cavity, although only one is stationary. For several flows, the fluid renewal rate is important to keep the quality of the fluid; in other words, the stationary apparent unyielded zones can be an issue. To account for this effect, Fig. 5 shows the displacement efficiency adopting two different approachs: the blue lines represent the displacement efficiency that computes all the apparent unyielded zones, as defined by Eq. 12, and the red lines represent the non-stationary displacement efficiency (Φ_{sta}), that computes only the stationary apparent unyielded zones. For low *Re* numbers ($Re < 10$ for $Pl = 0.4$ and $Re < 20$ for $Pl = 0.6$), there is no recirculation zone, and both displacement efficiencies have the same value. For the Stokes flow ($Re = 0.1$), the inertial forces are negligible and the flow exhibits a symmetric behavior

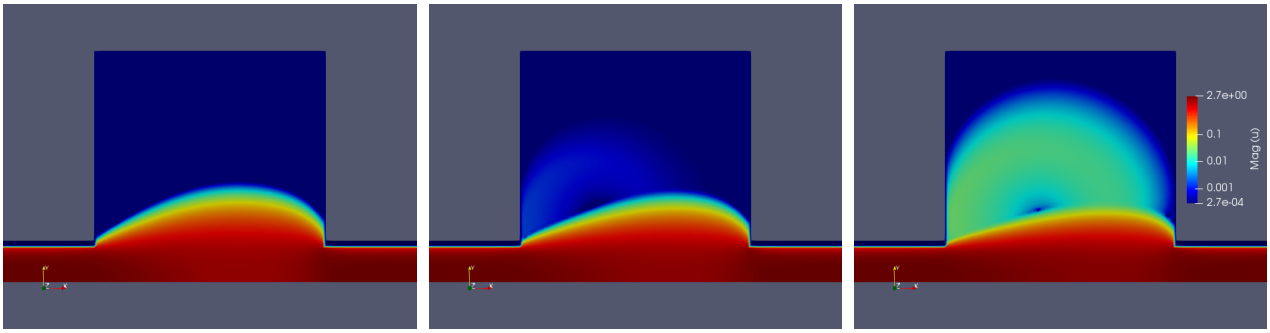

(a) *Re*=10 (b) *Re*=15 (c) *Re*=20

Figure 3. Dimensionless velocity magnitude inside the cavity for $Pl = 0.4$ and (a) $Re = 10$; (b) $Re = 15$; (c) $Re = 20$. All figures shares the same scale.

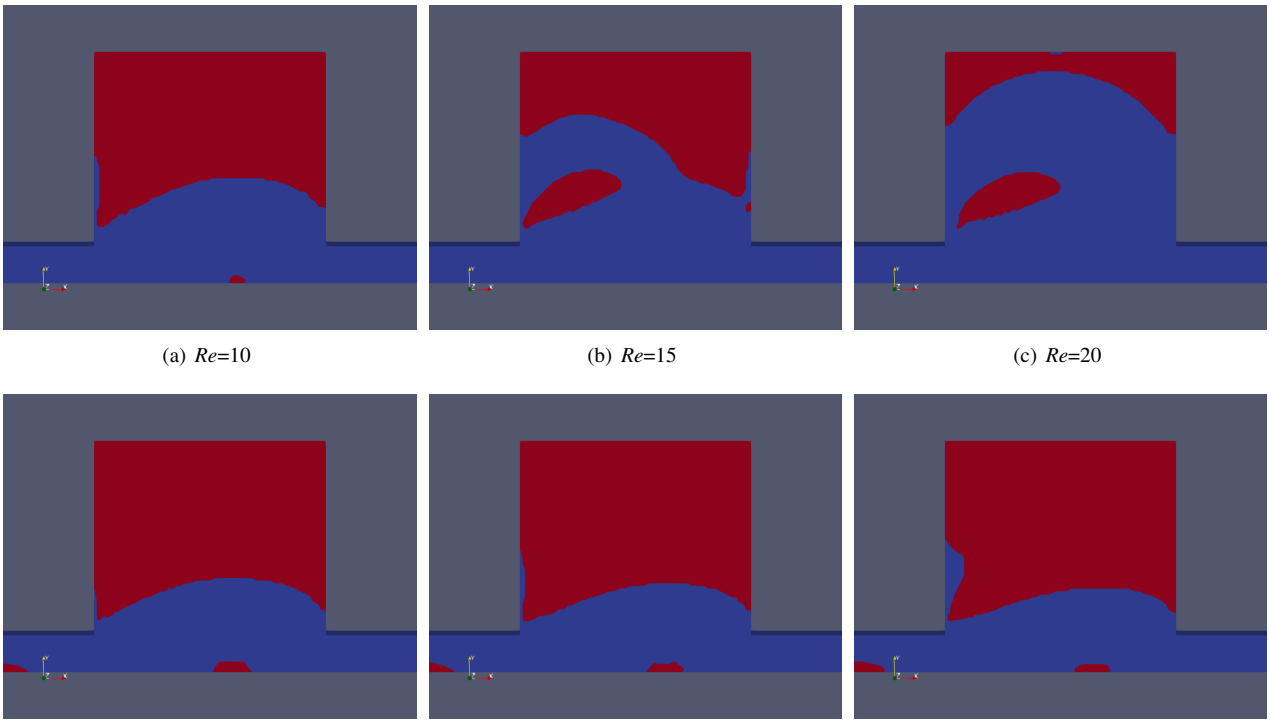

(a) *Re*=10 (b) *Re*=15 (c) *Re*=20

(d) *Re*=10 (e) *Re*=15 (f) *Re*=20

Figure 4. Apparent unyielded zones (red) and yielded zones (blue) for $Pl = 0.4$, in the firt line, and $Pl = 0.6$, in the second line.

in relation to the y^* axis. Increasing the Re, this symmetry is broken, and the flow leans towards the outlet channel, as can be seen in Fig. 3. This tilting increases the apparent unyielded zone inside the cavity, decreasing the displacement efficiency. This behavior is the opposite of the overall trend, where the displacement efficiency increases with the increase of the Reynolds number, particularly because of the effects of the recirculation zone. The plateau of the non-stationary displacement efficiency from $Re = 30$ to $Re = 50$ for $Pl = 0.4$ indicates that the recirculation zone have reached its maximum size. The displacement efficiency does not show the same behavior, because the apparent unyielded zone at the vortex center is still changing at this range of Reynolds numbers. As a higher plastic number means a more relevant viscoplastic behavior, the increase for $Pl = 0.4$ to $Pl = 0.6$ decreases both displacement efficiencies.

Figure 6 shows how the Nusselt number is influenced by the Reynolds number. Low Reynolds numbers favor the conduction heat transfer, so lower Nusselt numbers are expected. The emergence of the recirculation zone enhances the interaction between the channel and the cavity, which increases the Nusselt number. Therefore, it is possible to identify two major trendings in the Nusselt number: it have a natural trend to increase with the increase of the Reynolds number, and this tendency is enhanced when there is a recirculation zone inside the cavity. Figure 7 shows the dimensionless temperature profile over the axis y^* for $Pl = 0.4$. The presence of a recirculation zone can create a plateau of temperature inside the cavity. As Fig. 3(b) shows, there is a recirculation zone inside the cavity for $Re > 15$ and $Pl = 0.4$, but the plateau is only clear at Fig. 7 for $Re = 30$. Not only the size and position of the the recirculation zone explain this

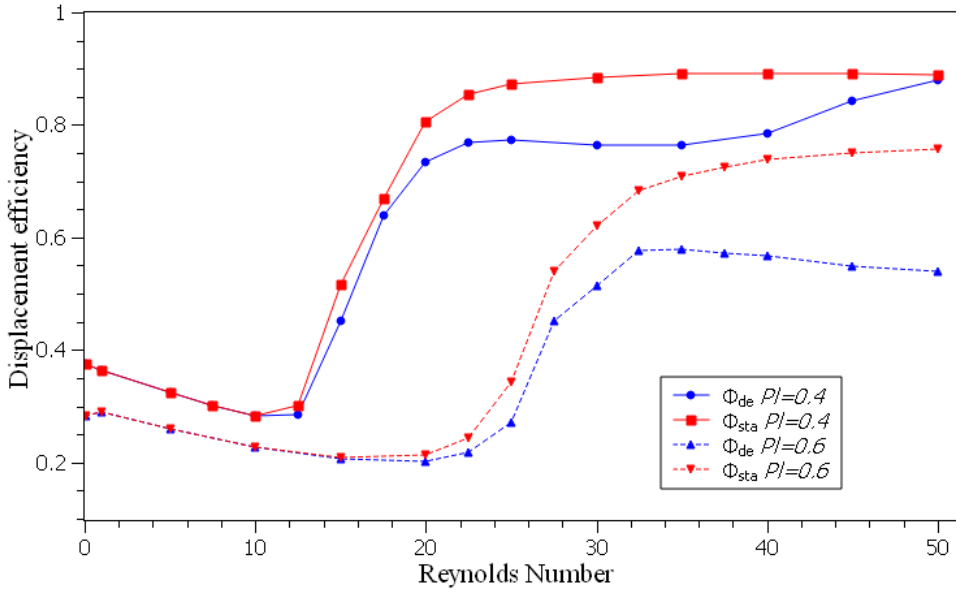

Figure 5. Displacement efficiency (Φ_{de}) and non-stationary displacement efficiency (Φ_{sta}) for 0.1$\leq$ *Re*$\leq$50, with $Pl = 0.4$ and $Pl = 0.6$.

difference, but the flow intensity of the recirculation zone also plays its role. The heat transfer by convection is increased with the intensification of the flow inside the cavity, and the plateau is more easily identifiable. Although the simulation with $Re = 0.1$ have the lowest Nusselt number, this flow has the highest dimensionless temperatures over all the profile. The lower inertia forces favor the conduction heat transfer and decreases the overall heat exchange. The increase of the plastic number from 0.4 to 0.6 decreases the mean Nusselt number as it increases the apparent unyielded zones.

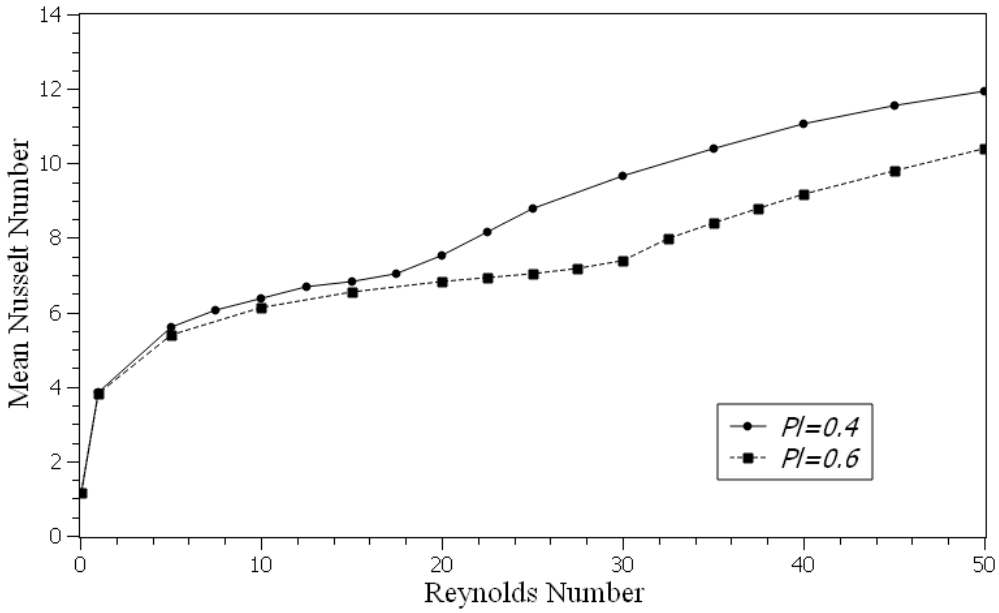

Figure 6. Mean Nusselt number for 0.1$\leq$ *Re*$\leq$50with $Pl = 0.4$.

The results for Hl can be found at Fig. 8. When the inertia forces are low, the head loss is high and positive, meaning that the channel with a cavity have a lower pressure drop when compared with a simple channel. This was expected as a wider channel offer less resistance to the flow. When the Reynolds number is increased, the relevance of the viscous forces decrease, decreasing the influence of the cavity over the flow when compared with a simple channel, although the head loss is still positive, meaning that the cavity channel still has a lower pressure drop than the simple channel.

Comparing the results of Fig. 6 and Fig. 8, it is clear that applications with heat transfer with this kind of geometry need an optimization procedure, as the heat transfer and the head loss have opposite trends in relation to the Reynolds

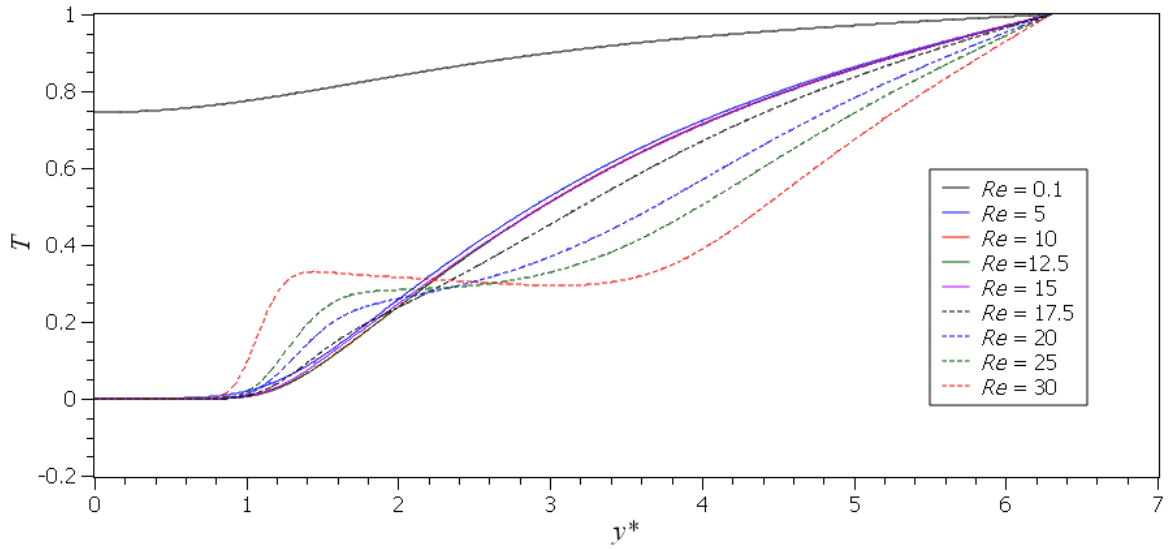

Figure 7. Dimensionless temperature profile at the axis y^* for 0.1$\leq$ *Re*$\leq$50, with $Pl = 0.4$.

number. As there is no evidence of effect of the recirculation zone over Hl at Fig. 8, theoretically the solution with the best efficiency would be a configuration that favor the emergence of a recirculation zone for low Reynolds, increasing the heat transfer without a significant increase in the pressure loss.

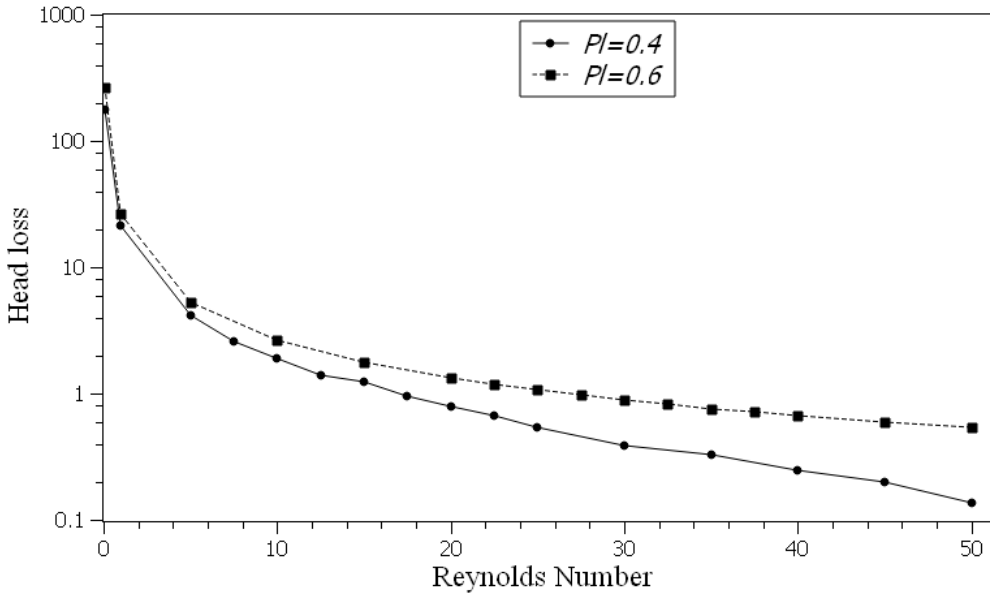

Figure 8. Head loss for 0.1$\leq$ *Re*$\leq$50, with $Pl = 0.4$ and $Pl = 0.6$.

4. FINAL REMARKS

The present study showed an analysis of the effect of the Reynolds number over a flow inside an planar expansion-contraction channel, obtained with an OpenFOAM® routine developed by the authors. The adopted plastic numbers were 0.4 and 0.6, while the others dimensionless groups were fixed as: $Pr = 14.0164$; $J = 10^4$; $n = 0.5$; $\eta^*_{\text{inf}} = 0.01$. The Reynolds number was varied from 0.1 to 50. For this configuration, a recirculation zone is able to surpass the yield stress limit when $Re \geq 15$ for $Pl = 0.4$ and when $Re \geq 25$ for $Pl = 0.6$, and this flow structure have a major impact over the temperature, the velocity profile, the displacement efficiency and Nusselt number, but there is no evidence of influence over the head loss.

For the studied range of Reynolds number, the Nusselt number have a positive dependence with *Re* particularly when the recirculation zone is formed. Lower Reynolds numbers have shown lower Nusselt numbers and higher temperatures

over the y^* axis.

For low Reynolds numbers, the displacement efficiency has a negative dependence with the *Re*, because of the loss of the flow symmetry. But when the recirculation zone is present, its effects are predominant and the displacement efficiency increases until a maximum defined by the size of the cavity. The head loss has a monotonic trend to decrease with the increase of Reynolds number, showing that the pressure drop in the channel with the cavity is increasing when compared to the pressure drop inside a simple channel.

5. ACKNOWLEDGEMENTS

The authors would like to thank the postgraduate program in mechanical engineering from the Federal University of Uberlândia and CAPES (Brazilian Graduate Education Foundation) for providing the necessary resources to the development of this work, including the scholarships of Luiz Paulo Borges Miranda, provided by CAPES.

6. REFERENCES

Celik, I.B., 2008. "Procedure for estimation and reporting of discretization error in cfd applications". *Journal of Fluids Engineering*, Vol. 130, No. 7, p. 078001.

de Souza Mendes, P.R., Naccache, M.F., Varges, P.R. and Marchesini, F.H., 2007. "Flow of viscoplastic liquids through axisymmetric expansions-contractions". *Journal of Non-Newtonian Fluid Mechanics*, Vol. 142, pp. 207–217.

de Souza Mendes, P.R. and Dutra, E.S.S., 2004. "Viscosity function for yield-stress liquids". *Applied Rheology*, Vol. 14, pp. 296–302.

Gupta, A.K., Mishra, P. and Chhabra, R.P., 2017. "Momentum and heat transfer characteristics of a thin circular disk in bingham plastic fluids". *Numerical Heat Transfer, Part A: Applications*, Vol. 72, No. 11, pp. 844–868.

Hermany, L., 2012. *Aproximações estabilizadas de escoamentos de fluidos viscoplásticos através de uma expansão seguida de uma contração axissimétrica*. Master's thesis, Universidade Federal do Rio Grande do Sul. Escola de Engenharia. Programa de Pós-Graduação em Engenharia Mecânica.

Naccache, M.F. and Barbosa, R.S., 2007. "Creeping flow of viscoplastic materials through a planar expansion followed by a contraction". *Mechanics Research Communications*, Vol. 34, No. 5-6, pp. 423–431.

Nirmalkar, N., Bose, A. and Chhabra, R.P., 2014. "Free convection from a heated circular cylinder in Bingham plastic fluids". *International Journal of Thermal Sciences*, Vol. 83, pp. 33–44.

Raja, A.H., Patel, S.A. and Chhabra, R.P., 2015. "Laminar forced convection heat transfer from a two-dimensional transverse plate in Bingham plastic fluids". *International Journal of Heat and Mass Transfer*, Vol. 83, pp. 690–709.

Shyam, R. and Chhabra, R.P., 2013. "Effect of prandtl number on heat transfer from tandem square cylinders immersed in power-law fluids in the low reynolds number regime". *International Journal of Heat and Mass Transfer*, Vol. 57, pp. 742–755.

Thompson, R.L. and Soares, E.J., 2016. "Viscoplastic dimensionless numbers". *Journal of Non-Newtonian Fluid Mechanics*, Vol. 238, pp. 57–64.

Turan, O., Poole, R.J. and N. Chakraborty, N., 2011. "Aspect ratio effects in laminar natural convection of Bingham fluids in rectangular enclosures with differentially heated side walls". *Journal of Non-Newtonian Fluid Mechanics*, Vol. 166, pp. 208–230.

7. RESPONSIBILITY NOTICE

The authors are the only responsible for the printed material included in this paper.